Hindawi
Mathematical Problems in Engineering
Volume 2022, Article ID 9577348, 16 pages
https://doi.org/10.1155/2022/9577348

Research Article

Unidirectional Geosynthetic Reinforcement Design for Bridging Localized Sinkholes in Transport Embankments

Peinan Li[1] **and Feng Su**[2]

[1]*College of Environmental Science and Engineering, Donghua University, Shanghai 201620, China*
[2]*Southwest Municipal Engineering Design & Research Institute of China, Chengdu, Sichuan 610000, China*

Correspondence should be addressed to Peinan Li; lipeinan_tj@163.com

Received 24 July 2021; Revised 8 December 2021; Accepted 15 January 2022; Published 12 February 2022

Academic Editor: Jose Renato de Sousa

The durability of foundations with localized sinkholes can be improved by geosynthetic-reinforced soil. Current design methods for geosynthetic-reinforced structures are based on the assumptions that the vertical load is distributed uniformly on the geosynthetic above the sinkhole and it corresponds to the geostatic stress in the anchorage area. In this study, a new analytical method is proposed to consider the 'secondary arching effect' and the vertical load distribution in the anchorage area due to the 'arching effect.' The influence of vertical load acting on the geosynthetic is analyzed based on three different cases. Results indicate that the increment of vertical load on the geosynthetic in the anchorage area has little effect on the maximum tensile force and surface settlement. Compared to a uniform load distribution on the geosynthetic above the sinkhole, the assumption of an inverse triangular load distribution can reduce the maximum tensile force and surface settlement. A new design method is proposed to determine the minimum geosynthetic stiffness to meet design standards. The obtained results verify the method as an applicable tool to meet the serviceability limit state and the ultimate limit state criteria.

1. Introduction

With the development of infrastructure in China, a massive number of highways and railways are built in karst areas. However, some underground cavities are neither readily detected nor do they appear after the construction of the roads, especially in the case of small cavities. Sinkholes usually result from the collapse of underground cavities. Transport routes are damaged when the underground cavities collapse suddenly. Therefore, it is necessary to reinforce roads to prevent localized sinkholes. Due to the cost-effectiveness and installation convenience, reinforcing embankments with geosynthetics is an attractive technique [1, 2, 3]. Reinforced soil can improve the service performance of buildings or infrastructure, consequently improving the toughness of urban structures.

Experimental studies [4, 5, 6, 7, 8] have indicated that geosynthetics, if properly selected, protect embankments from small cavities, and unidirectional geosynthetics with machine direction oriented along the direction of traffic are the most appropriate. Based on simple assumptions, geosynthetic shape, surface settlement, and tension within the geosynthetic can be calculated theoretically and design methods are proposed (BS8006 2010) [9, 10, 11].

The BS8006 (2010) design method is based on the tensioned membrane theory only. Combining tensioned membrane theory with arching theory, Giroud et al. [12] proposed a design method to span voids for soil layer-geosynthetic systems. Blivet et al. [13] adopted the 'RAFAEL' method to take the expansion of soil into account further, obtaining the relationship between surface settlement and geosynthetic deflection. These methods apply the tensioned theory to describe the membrane effect of the geosynthetic located above the cavity (implying the fixity of geosynthetic at the edge of the cavity). Villard and Briancon [7] considered the geosynthetic behaviors in the anchorage area and at the edge of the cavity.

A key issue is a load imposed on the geosynthetic. If the embankment is high enough, the 'arching effect' will occur within the embankment when the underground cavity underneath the embankment collapses. The vertical stress q acting on the portion of geosynthetic located above the sinkhole decreases and becomes smaller than the sum of the vertical geostatic stress (γH) and the surcharge q_s applied on the embankment surface ($q < \gamma H + q_s$). The vertical stress q_a acting on the portion of geosynthetic in the anchorage area increases and exceeds $\gamma H + q_s$. Most of the design methods considered the arching effect but none of them investigated the influence of the vertical load distribution on geosynthetic in the anchorage area owing to the arching effect. These design methods assume the uniform distribution of q; however, experiments reveal that q is not uniform [14, 15, 16, 17] for the nonuniform vertical displacement of the geosynthetic above the sinkhole.

To improve the current design methods, a new approach is developed. An inverse triangular distribution for q and a Gaussian distribution for q_a are applied based on experimental results [18, 19, 20, 21]. The influence of different distribution forms of q as well as q_a on the mobilized tension and surface settlement is analyzed using different methods. Finally, analytical formulations and design methods for long and circular voids are proposed.

2. Arching Effect

2.1. Vertical Load on the Geosynthetic in the Collapse Area. The stress transfer, owing to relative movement within the soil, is commonly defined as the arching effect [22]. Embankment fills and underlying geosynthetic layers are generally located on firm soils. The vertical stress then equates to the geostatic stress of the fills and surcharge. If sinkholes below the geosynthetic collapse (after the construction of the geosynthetic-reinforced embankment), as illustrated in Figure 1, the geosynthetic deflects and the relative movement within the soil occurs between collapse and anchorage areas subjected to a vertical load. A portion of the vertical stress on the geosynthetic in the collapse area transfers to the anchorage area. Thus, the vertical stress on the geosynthetic in the collapse area decreases. Based on the assumptions that the vertical load distributes uniformly and slip planes are vertical, the vertical load on the geosynthetic in the collapse area can be calculated using the Terzaghi method (1943).

For a long void of width B,

$$q = \frac{B(\gamma - 2c/B)}{2K\ \tan\varphi_u}\left(1 - e^{-K\tan\varphi_u 2H/B}\right) + q_s e^{-2K\tan\varphi_u H/B}. \quad (1)$$

For a circular void of diameter D,

$$q = \frac{D(\gamma - 4c/D)}{4K\ \tan\varphi_u}\left(1 - e^{-K\tan\varphi_u 4H/D}\right) + q_s e^{-4K\tan\varphi_u H/D}. \quad (2)$$

The load on the geosynthetic in the collapse area can be calculated conservatively for cohesive and cohesionless soils ($c = 0$), using (1) and (2) [21]. Experimental data indicates that the value of K is larger than 1 [19, 22, 23]. Some design methods indicate that K is replaced by the active Earth pressure coefficient K_a [13, 24, 25].

$$K_a = \tan^2\left(45^\circ - \frac{\varphi_u}{2}\right). \quad (3)$$

Since the deflection of the geosynthetic is not uniform, the vertical stress on geosynthetic above the sinkhole redistributes in response to relative displacement between fills above the sinkhole. The portions of the geosynthetic close to the edge of the sinkhole deflect less and bear more vertical loads. Sloan [14] defined this phenomenon as a 'secondary arching effect'. For the collapse area, an inverse triangular distribution is adopted to describe the stress redistribution on the geosynthetic [26].

The 'secondary arching effect' changes the distribution of vertical stress; however, the magnitude of the average load and the total vertical force Q on the geosynthetic in the collapse area do not undergo any changes. Thus, Q in the cases of cohesive and cohesionless soils can be approximately calculated by multiplying the vertical load by the loading area as given as follows.

Long void:

$$Q = qB = \frac{B^2(\gamma - 2c/B)}{2K_a\tan\varphi_u}\left(1 - e^{-K_a\tan\varphi_u 2H/B}\right) + Bq_s e^{-2K_a\tan\varphi_u H/B}. \quad (4)$$

Circular void:

$$Q = q\frac{\pi D^2}{4} = \frac{\pi D^3(\gamma - 4c/D)}{16K_a\tan\varphi_u}\left(1 - e^{-K_a\tan\varphi_u 4H/D}\right) + \frac{\pi D^2}{4}q_s e^{-4K_a\tan\varphi_u H/D}. \quad (5)$$

2.2. Vertical Load on the Geosynthetic in the Anchorage Area. Adachi et al. [18], Jia [19], and Gao [20] measured the vertical stress q_a on the fixed support through two-dimensional trapdoor experiments. The vertical stress on the fixed support increased when the trapdoor lowered. The Earth pressure increasing rate $(q_a - q_0)/q_0$ was used to represent the increment of q_a. Experimental data demonstrates that the Earth pressure increasing rate shows close correlations to the standardized distance from the pressure gauge to the centerline of the descending trapdoor by the width of the trapdoor (x/B) and the value of H/B. This experimental data is summarized in Figure 2. Figure 2 show that the value of $(q_a - q_0)/q_0$ decreases rapidly with the increment of x/B. The decrease of $(q_a - q_0)/q_0$ is more apparent with a smaller value of H/B. The relationship between $(q_a - q_0)/q_0$, x/B, and H/B can be approximately described by a Gaussian distribution function from Figure 2 as

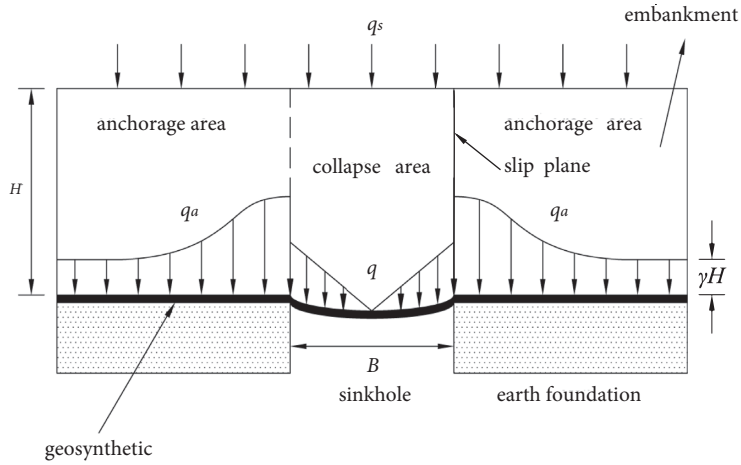

Figure 1: Vertical loads on the geosynthetic for a long void.

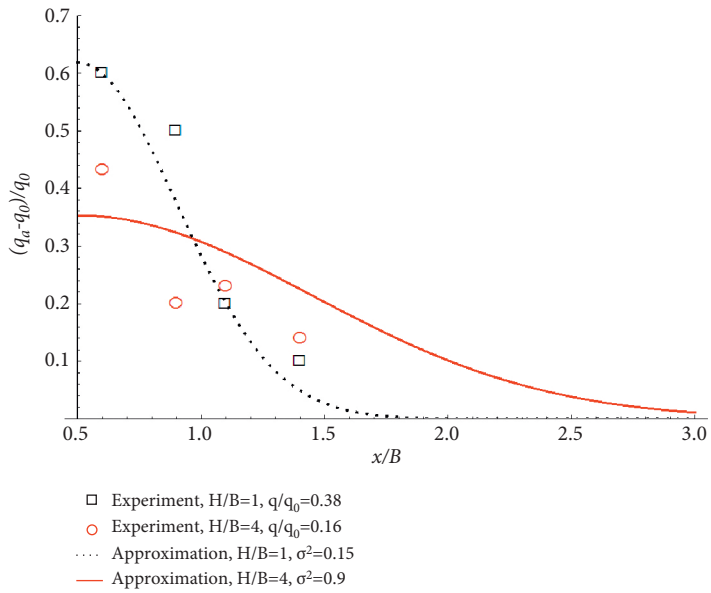

(a)

Figure 2: Continued.

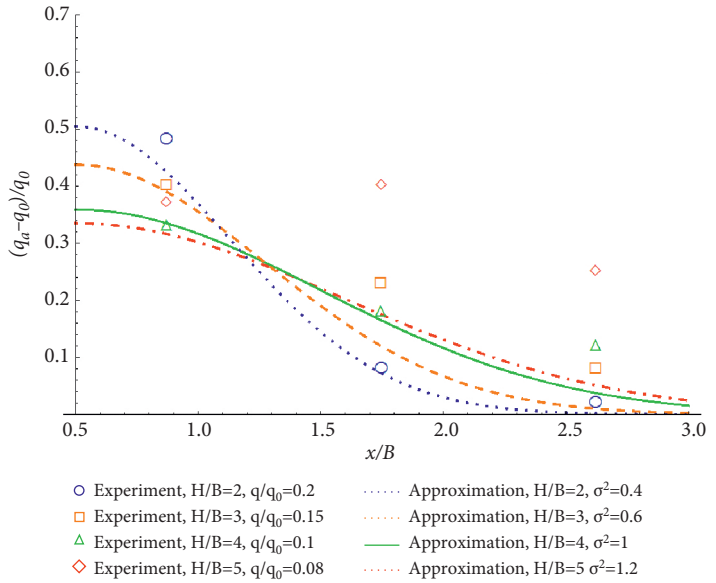

(b)

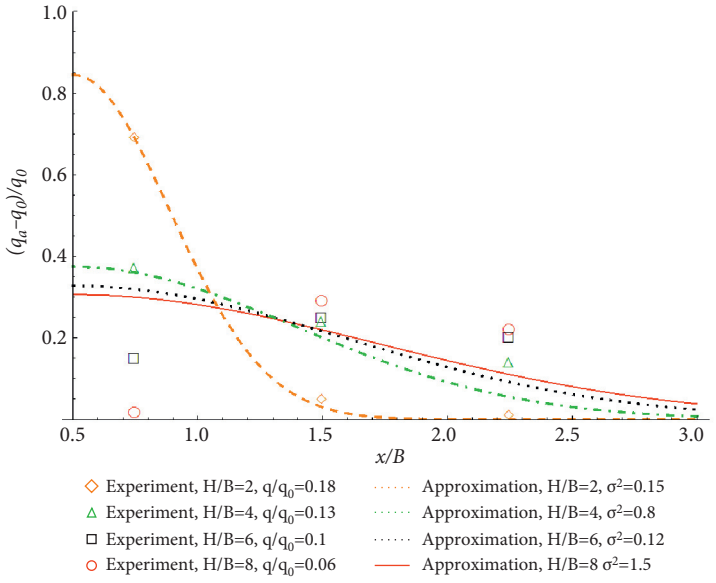

(c)

Figure 2: Comparison of the approximated and experimental results of the increments in Earth pressure outside the trapdoor. (a) Adichi (2003), (b) Jia (2007), and (c) Gao (2009).

$$\frac{(q_a - q_0)}{q_0} = a_1 \frac{1}{\sqrt{2\pi}\sigma} \exp\left[-\frac{(x/B - 0.5)^2}{2\sigma^2}\right]. \quad (6)$$

The vertical load on the fixed support can be calculated by

$$q_a = a \frac{1}{\sqrt{2\pi}\sigma} \exp\left[-\frac{(x/B - 0.5)^2}{2\sigma^2}\right] + q_0, \quad (7)$$

where σ is a function of H/B and the properties of the fills, $a_1 = a/q_0$, where a is a coefficient determined by

$$\int_{B/2}^{+\infty} [q_a - q_0] \mathrm{d}x = \frac{B}{2}(q_0 - q). \quad (8)$$

Thus,

$$a = q_0 - q. \quad (9)$$

Substituting (9) into the (7), the following expression is obtained.

$$q_a = (q_0 - q) \frac{1}{\sqrt{2\pi}\sigma} \exp\left[-\frac{(x/B - 0.5)^2}{2\sigma^2}\right] + q_0. \quad (10)$$

Both the experimental results and the estimated results are illustrated in Figure 2. The smaller the value of H/B is, the better agreement between the approximate results and the experimental data will be. Furthermore, there is a great difference between experimental and estimated results if H/B >4. Therefore, for long voids and H/B =1–4, the vertical load on geosynthetic in the anchorage area can be estimated by the proposed equation with the proper value of σ.

3. Analysis of Reinforced Embankment Bridging a Long Void

3.1. Geosynthetic Behavior in the Collapse Area. The behavior of the geosynthetic is assumed to be linear elastic: $T = J\varepsilon$. Half of the void is taken into consideration. The frictional forces between the fills and the geosynthetic in the collapse area are neglected.

Considering an infinitesimal element dx of the geosynthetic in the collapse area (Figure 3), the equilibrium equations of vertical and horizontal forces give

$$q(x) = \frac{\mathrm{d}T_V}{\mathrm{d}x}, \tag{11}$$

$$\mathrm{d}T_H = 0, \tag{12}$$

For an infinitesimal element dx,

$$T_V = -T_H \frac{\mathrm{d}z}{\mathrm{d}x}. \tag{13}$$

Thus,

$$\frac{\mathrm{d}T_V}{\mathrm{d}x} = -\frac{\mathrm{d}T_H}{\mathrm{d}x}\frac{\mathrm{d}z}{\mathrm{d}x} - T_H\frac{\mathrm{d}^2 z}{\mathrm{d}x^2}. \tag{14}$$

Combining equations (11), (12), and (14), the following expression is obtained.

$$\frac{q(x)}{T_H} = -\frac{\mathrm{d}^2 z}{\mathrm{d}x^2}. \tag{15}$$

Inverse triangular load distribution on the geosynthetic in the collapse area is given.

$$q(x) = \frac{4Q}{B^2}x. \tag{16}$$

Combining (15) and (16), the following expression is obtained.

$$\frac{4Q}{T_H B^2}x = -\frac{\mathrm{d}^2 z}{\mathrm{d}x^2}. \tag{17}$$

Solving (17) subjected to the boundary conditions that $z = 0$ for $x = B/2$ and $z' = 0$ for $x = 0$, one can obtain

$$z = -\frac{2Q}{3T_H B^2}x^3 + \frac{QB}{12T_H}. \tag{18}$$

At the edge of the cavity (point A), the tensile force within the geosynthetic reaches the maximum value T_1.

$$T_1 = \sqrt{{T_H}^2 + \left(\frac{Q^2}{4}\right)}. \tag{19}$$

Substituting $x = 0$ into (18), the geosynthetic deflection w can be written as

$$w = \frac{QB}{12T_H}. \tag{20}$$

Using (18), the increase in geosynthetic length ΔL on the half-width of the cavity can be calculated as follows:

$$\begin{aligned}\Delta L &= \int \mathrm{d}s - \frac{B}{2} \\ &= \int_0^{B/2} \sqrt{1 + (z')^2}\,\mathrm{d}x - \frac{B}{2} \\ &= -\frac{B}{2} + \frac{1}{12}B\left[\sqrt{4 + \frac{Q^2}{{T_H}^2}} + 4M\left(-\frac{Q^2}{4{T_H}^2}\right)\right].\end{aligned} \tag{21}$$

where $M(-t)$ is a hypergeometric function in the Wolfram Mathematica package, which can be expanded by the Maclurin series as

$$M(-t) = 1 - \frac{t}{10} + \frac{t^2}{24} - \frac{5t^3}{208} + \frac{35t^4}{2176} - \frac{3t^5}{256} + \frac{231t^6}{25600} - \frac{429t^7}{59392} + \frac{195t^8}{32768} + O(t)^9. \tag{22}$$

The first three Maclurin series terms of $M(-t)$ are precise enough under the situation that $Q/(2T_H) < 1$ for $w/B < 1/6$. Equation (21) can be rewritten as

$$\Delta L = -\frac{B}{2} + \frac{1}{12}B\left(\sqrt{4 + \frac{Q^2}{{T_H}^2}} + 4 - \frac{Q^2}{10{T_H}^2} + \frac{Q^4}{96{T_H}^4}\right). \tag{23}$$

The geosynthetic tension deformation χ on the half-width of the cavity can be calculated as follows:

$$\begin{aligned}\chi &= \int \varepsilon \mathrm{d}s = \int_0^{B/2} \varepsilon\sqrt{1 + (z')^2}\,\mathrm{d}x \\ &= \frac{T_H}{J}\left(\frac{B}{2} + \frac{BQ^2}{40{T_H}^2}\right).\end{aligned} \tag{24}$$

Combining (23) and (24), the displacement of point A U_A can be written as

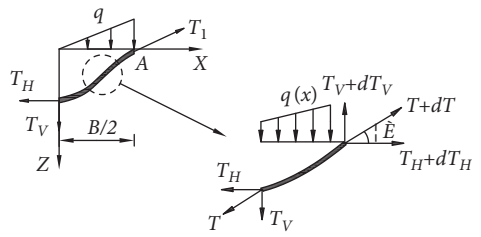

Figure 3: Schematic diagram of forces within the geosynthetic in the collapse area.

$$U_A = \Delta L - \chi = -\frac{B}{2} + \frac{1}{12}B\left(\sqrt{4 + \frac{Q^2}{{T_H}^2}} - \frac{Q^2}{10{T_H}^2} + \frac{Q^4}{96{T_H}^4}\right) - \frac{T_H}{J}\left(\frac{B}{2} + \frac{BQ^2}{40{T_H}^2}\right). \quad (25)$$

3.2. Surface Settlement. In Figure 4, the subsidence will rise rapidly to the surface of the embankment when the geosynthetic deflects. The soil above the void expands in volume thus indicating dilation. Thus, surface displacement is less than geosynthetic displacement in the vertical direction. Assuming that the shape of surface settlements and the geosynthetic sag are the same (cubical parabola) which is just a first approximation, combined with (20), the relation among surface settlement w_s, deflection of geosynthetics w, soil expansion coefficient C_e, and height of the fill H can be obtained [6, 24, 27]:

$$w_s = w\left(1 - \frac{18T_H}{Q}\frac{H}{B}\left(C_e - 1\right)\right). \quad (26)$$

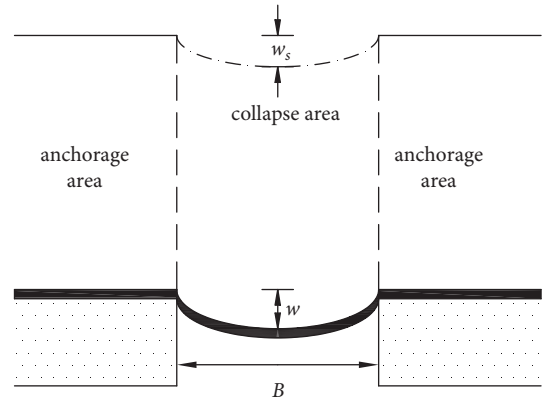

Figure 4: Schematic diagram of the surface settlement.

3.3. Geosynthetic Behavior in the Anchorage Area. The friction laws at the soil/geosynthetic interfaces are supposed to be the Coulomb friction law in Figure 5. In Figure 6, the tensile force within the geosynthetic decreases from T_1 to T_2 at the edge of the cavity based on the limit equilibrium of segment of geosynthetic sheet acting by friction on a circular arc (7) and (27).

$$T_2 = T_1 e^{-\beta k_0 \alpha \tan\varphi_1}, \quad (27)$$

where $k_0 = 1$ for $U_A \geq U_0$, $k_0 = U_A/U_0$ for $U_A < U_0$; and $\tan\beta = |z'(B/2)| = Q/(2T_H)$.

In Figure 7, the geosynthetic AC in the anchorage area is divided into n elements evenly, and the length of each element equals Δx. A horizontal stress is caused by the friction between the geotextile and the upper layer; however, the influence is not very high, so this horizontal stress can be neglected. Thus, the shear stress on the upper and lower interfaces at any element of the geosynthetic is expressed as

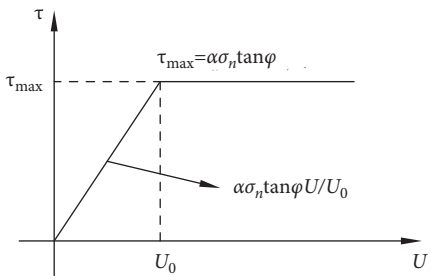

Figure 5: Coulomb friction law.

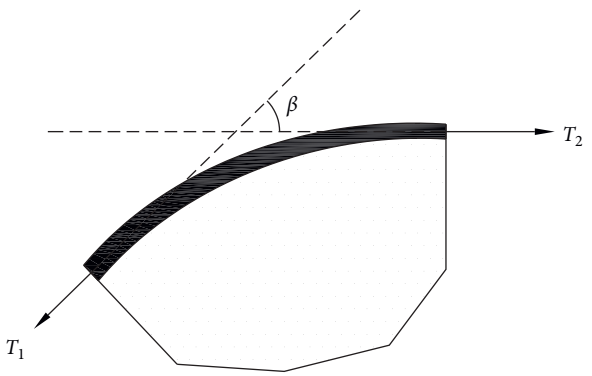

Figure 6: Edge of the void.

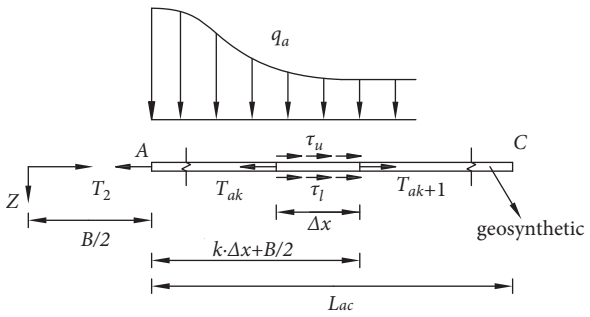

Figure 7: Schematic diagram of the forces within the geosynthetic in the anchorage area.

$$\tau_u = K_U q_a \alpha \tan\varphi_u,$$
$$\tau_l = K_U q_a \alpha \tan\varphi_l, \tag{28}$$

where $K_U = 1$ for $U_{ak} \geq U_0$ or $K_U = U_{ak}/U_0$ for $U_{ak} < U_0$.

The equilibrium of the element k is expressed as

$$T_{ak+1} = T_{ak} - K_U q_a \alpha (\tan\varphi_u + \tan\varphi_l)\Delta x, \tag{29}$$

$$U_{ak+1} = U_{ak} - \frac{T_{ak+1}}{J}\Delta x. \tag{30}$$

The equilibrium of the point A ($k = 0$) is given as

$$T_2 = T_{a0}, U_A = U_{a0}. \tag{31}$$

At the end of the geosynthetic (point C), the tensile force within the geosynthetic equals 0; that is,

$$T_{ak}|_{k \longrightarrow n} = T_{ac} = 0. \tag{32}$$

Combining equations (29) and (30) with the boundary conditions that $T_{ac} = 0$, $T_{a0} = T_2$ and $U_A = U_{a0}$, the system can be solved by an iterative calculation with the following equations.

$$\begin{cases} T_{ak+1} = T_{ak} - K_U q_a \alpha (\tan\varphi_u + \tan\varphi_l)\Delta x, \\ \\ U_{ak+1} = U_{ak} - \dfrac{T_{ak+1}}{J}\Delta x. \end{cases} \tag{33}$$

3.4. Determination of T_1 and w_s Based on an Example. To be more specific, an example is taken herein to elaborate the calculation procedure of the maximum tensile force and surface settlement. The relevant parameters used in the calculation example are given in Table 1.

From equations (1), (3), and (4), we obtain $q = 56$ kPa and $Q = 112$ kN. Let $q_0 = 280$ kPa; the value of q/q_0 is 0.2. Based on Figure 2(b), σ^2 is assumed to be 0.4. From equations (10), (19), and (25), we can obtain

Table 1: Parameters in the calculation example.

Parameter	Value
Cavity width (B)	2 (m)
Fill soil thickness (H)	4 (m)
Internal friction angle of the fill soil (φ_l)	35 (°)
Internal friction angle of the foundation soil(φ_u)	35 (°)
Unit weight of fill soil (γ)	20 (kN/m^3)
Displacement of the geosynthetic at the point a (U_0)	10 (mm)
Frictional coefficient (α)	0.9
Expansion coefficient of the fill soil (C_e)	1.04
Anchorage length (L_{ac})	3 (m)
Vertical overload applied on the fill soil surface (q_s)	0

$$q_a = 15 \exp\left[-\frac{(x/2 - 0.5)^2}{0.8}\right] + 280,$$

$$T_1 = \sqrt{T_H^2 + 3136},$$

$$U_A = -\frac{1}{3} + \frac{1}{6}\left(\sqrt{4 + \frac{112^2}{T_H^2} - \frac{112^2}{10T_H^2} + \frac{112^4}{96T_H^4}}\right) - \frac{T_H}{2000}\left(1 + \frac{627}{T_H^2}\right). \tag{34}$$

Let $\Delta x = 0.001$ m. From (33) with $T_{a0} = T_2$ and $U_A = U_{a0}$, the relationship between T_{ac} and T_H is obtained in Figure 8. When $T_{ac} = 0$, we obtain $T_H = 74.7$ kN/m and $T_1 = 93$ kN/m.

Combining (20) and (26), we obtain $w_s = 37$ mm.

3.5. Influence of Vertical Loads Applied to the Geosynthetic. To investigate the influence of the form of vertical load distribution and the increment of vertical load in the anchorage area on the maximum tensile force and surface settlement, three calculation models are adopted for comparison.

Model 1: an inverse triangular load distribution on the geosynthetic in the collapse area and a Gaussian load distribution on the anchorage area (Figure 9(a)).

Model 2: an inverse triangular load distribution on the geosynthetic in the collapse area and a uniform load distribution on the anchorage area (Figure 9(b)).

Model 3: a uniform load distribution on the geosynthetic in the collapse area and anchorage area (Figure 9(c)).

Figures 10, 11, 12, 13, 14, 15, and 16 illustrate the variation tendency of the maximum tensile force and surface settlement against various parameters. From the holistic perspective, the same variation tendency of the maximum tensile force and surface settlement can be observed from these three models in Figures 10–16. It can be seen that the surface settlement calculated by model 1 is the lowest and the maximum tensile force calculated by model 2 is the smallest. Apart from that, compared with a uniform load distribution on the geosynthetic in the collapse area in model 3, an inverse triangular load distribution used in model 1 and model 2 induces much smaller maximum tensile force and surface settlement,

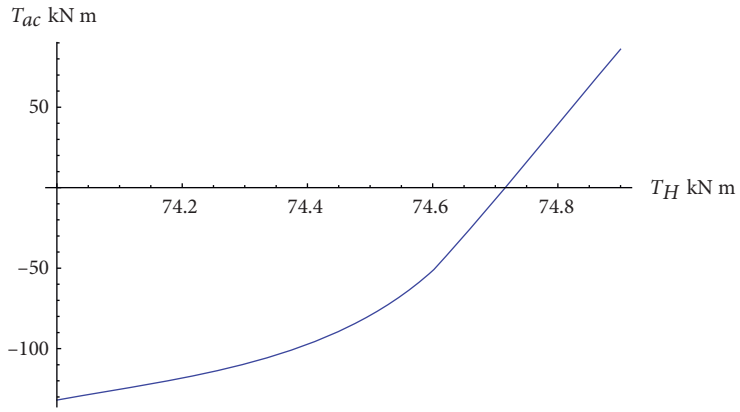

Figure 8: Relationship between T_{ac} and T_H.

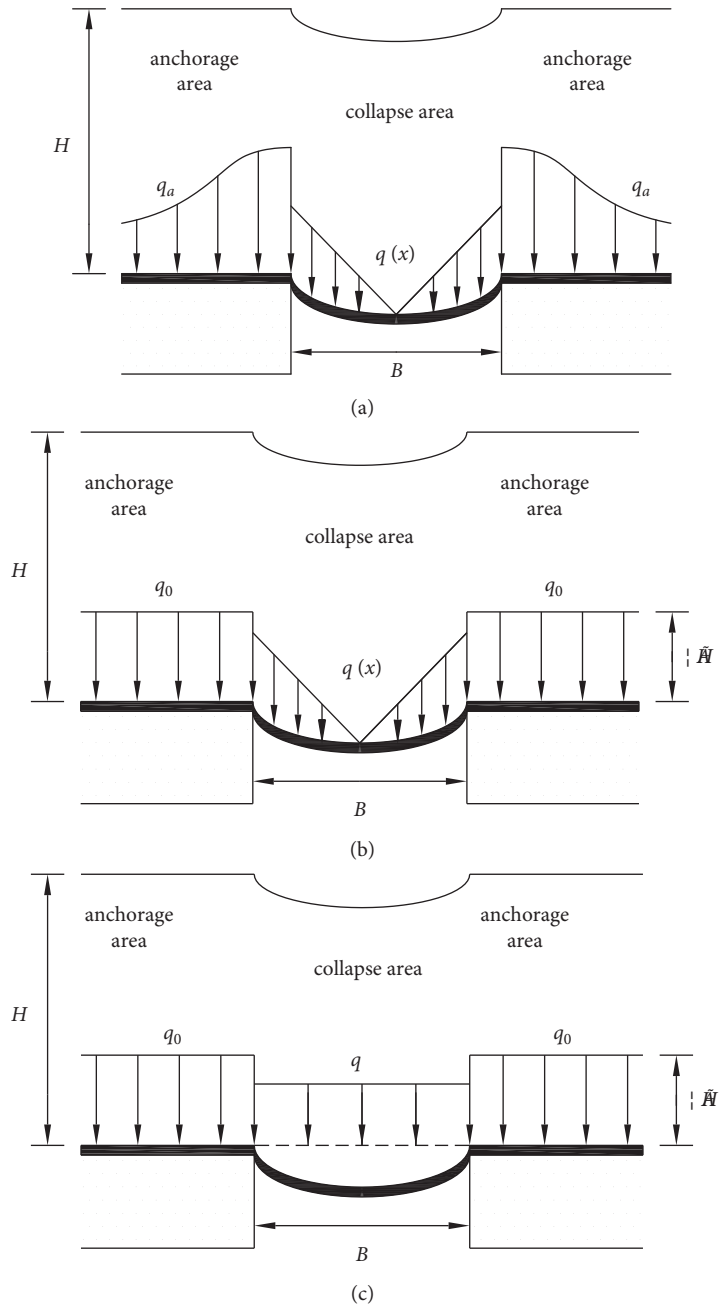

Figure 9: Schematic diagram of the vertical loads on geosynthetics for three calculation models: (a) model 1, (b) model 2, and (c) model 3.

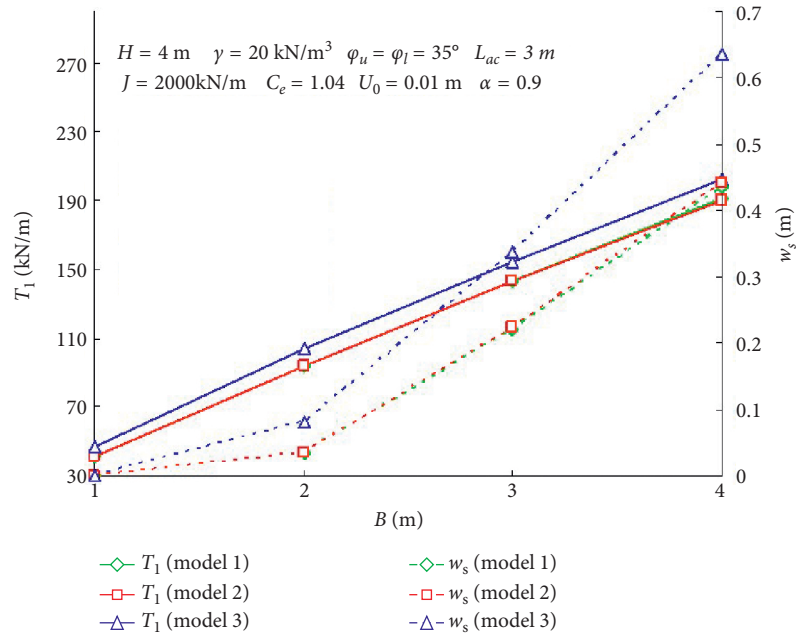

Figure 10: Influence of the width of the void on the maximum tensile force and surface settlement.

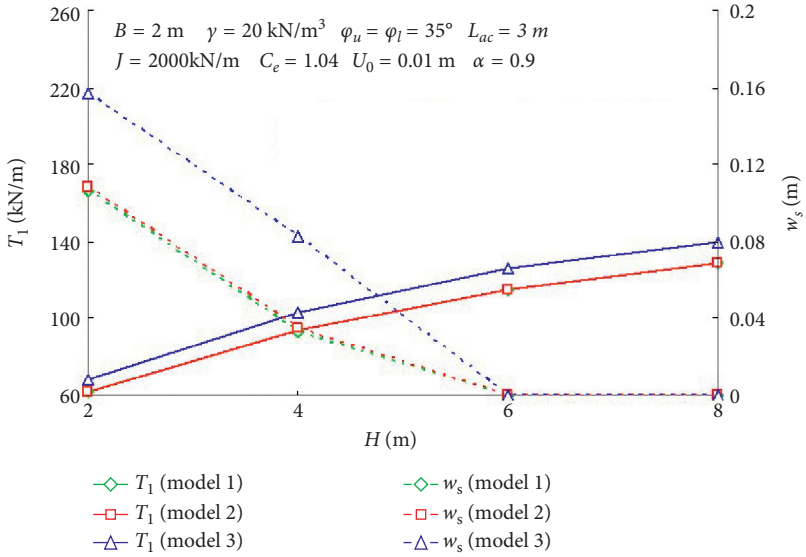

Figure 11: Influence of the height of the embankment on the maximum tensile force and surface settlement.

indicating that a uniform load distribution in the collapse area will overestimate the tensile force of geosynthetic and surface settlement of the embankment. Meanwhile, the vertical stress at the edge of the void in model 1 is larger than that in model 2 because of different load distributions in the anchorage area used in these two models. Generally, large vertical stress at the edge of the void will lead to less elongation of the geotextile. In consequence, a smaller surface settlement in model 1 should be observed. Unexpectedly, calculation results show that little discrepancy exists, which means the increment of vertical stress in the anchorage area due to the 'arching effect' has little effect on both tensile force and surface settlement. Hence, model 2 is considered the best calculation model for its accuracy and simplicity.

From the perspective of different parameters, all parameters are insensitive to the load distribution on the geosynthetic in the anchorage area but susceptible to the load distribution on the geosynthetic in the collapse area, which demonstrates the importance of the form of load distribution in the collapse area in practical engineering. As expected, Figure 10 shows that the size of cavity B has the most significant effect on the maximum tensile force and surface settlement. Therefore, it requires that the size of the underground cavity should be known as precisely as possible. It can

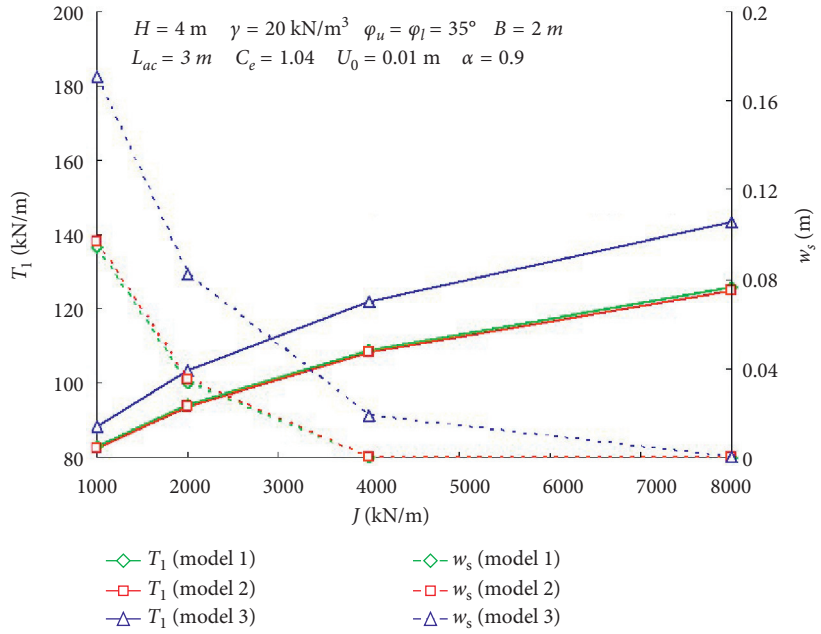

Figure 12: Influence of the tensile stiffness of the geosynthetic on the maximum tensile force and surface settlement.

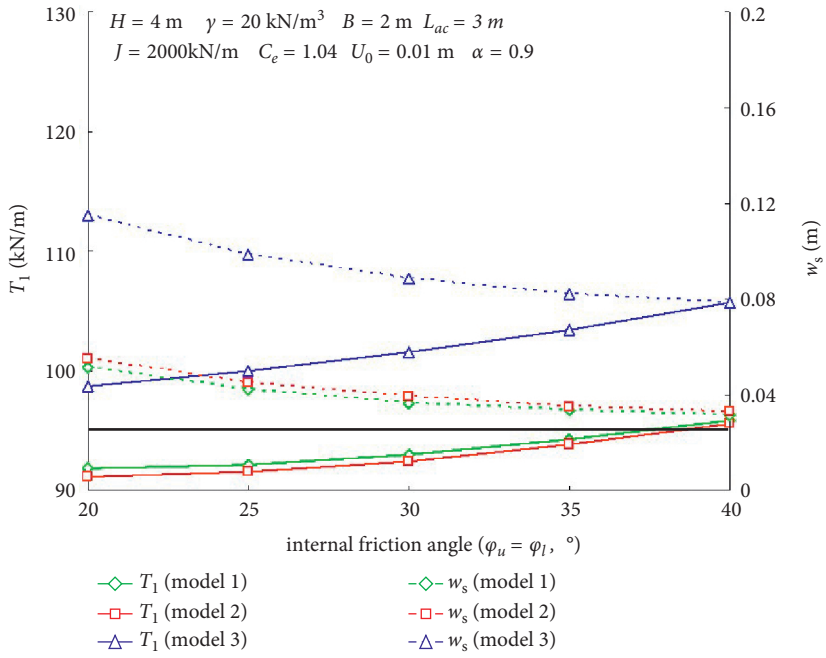

Figure 13: Influence of the internal friction angle on the maximum tensile force and surface settlement.

be seen from Figures 11–14 that the maximum tensile force and the maximum surface settlement have the opposite trends as an increase in the height of embankment H, the tensile stiffness of the geosynthetic J, internal friction angle φ_u, and relative displacement U_0, respectively. Furthermore, φ_u and U_0 have little effect on the tensile force and surface settlement, compared to H and J. Figure 15 indicates that the anchorage length L_{ac} has no effect on the maximum tensile force and surface settlement when L_{ac} exceeds 1 m. Hence, the influence of the anchorage length can be neglected for that the anchorage length is long enough in practice. In spite of difficult determination to the expansion coefficient α in practice, the results indicate that α only affects the surface settlement. Consequently, the maximum tensile force remains constant

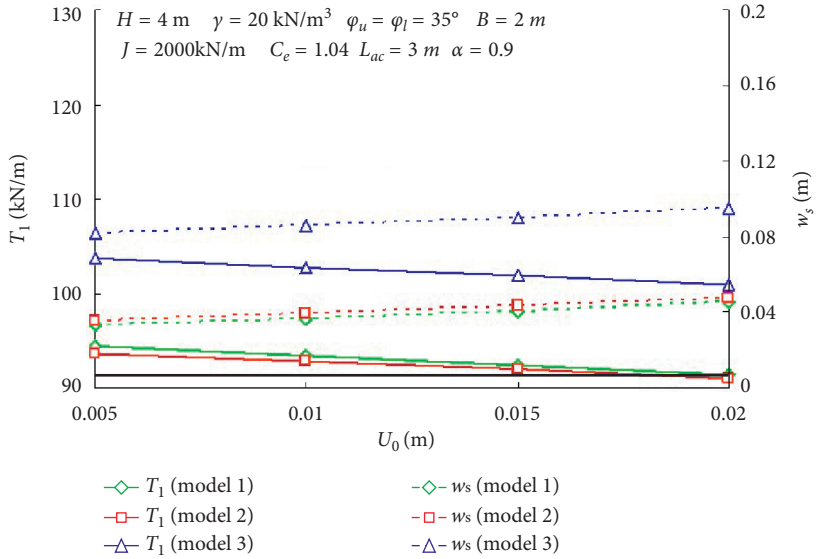

Figure 14: Influence of U_0 on the maximum tensile force and surface settlement.

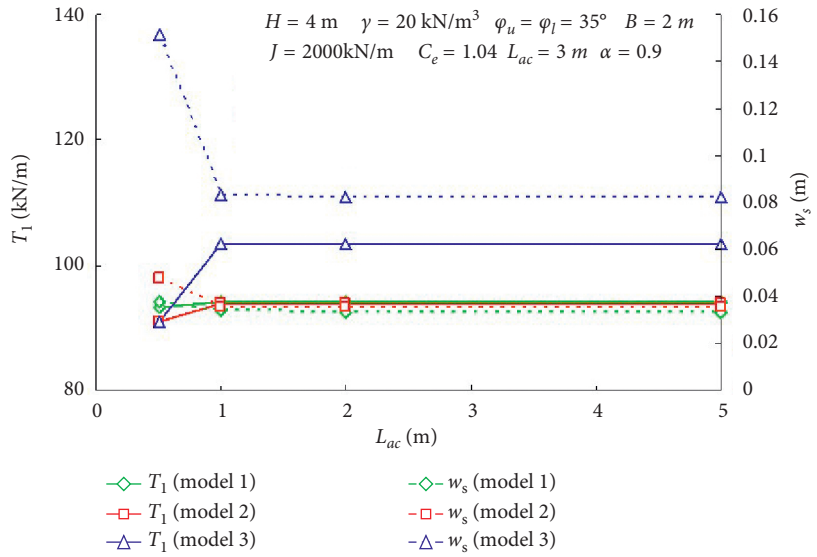

Figure 15: Influence of L_{ac} on the maximum tensile force and surface settlement.

and an increase in α involves a decrease in the maximum surface settlement, as shown in Figure 16.

3.6. Analytical Formulation. Based on the analysis above, the vertical stress on geosynthetic in the anchorage area can be simplified with the initial uniform load q_0 instead of a Gaussian load distribution.

Thus, the analysis of geosynthetic in the anchorage can be simplified with Briancon's method [23].

$$\begin{cases} \text{if } U_A \le U_0 : \; U_A = \dfrac{T_2}{Jr}, \\ \text{if } U_A > U_0 : \; U_A = U_0 + \dfrac{T_2^{\,2} - T_0^{\,2}}{2J\tau_0}. \end{cases} \tag{35}$$

With $\tau_0 = \alpha q_0 (\tan\varphi_u + \tan\varphi_l)$, $r^2 = \tau_0/(JU_0)$, and $T_0 = JrU_0$, $T_2 = \sqrt{T_H^{\,2} + Q^2/4}/e^{\beta k_0 \alpha \tan\varphi_l}$.

Combining (25) and (35), the solution of the system is

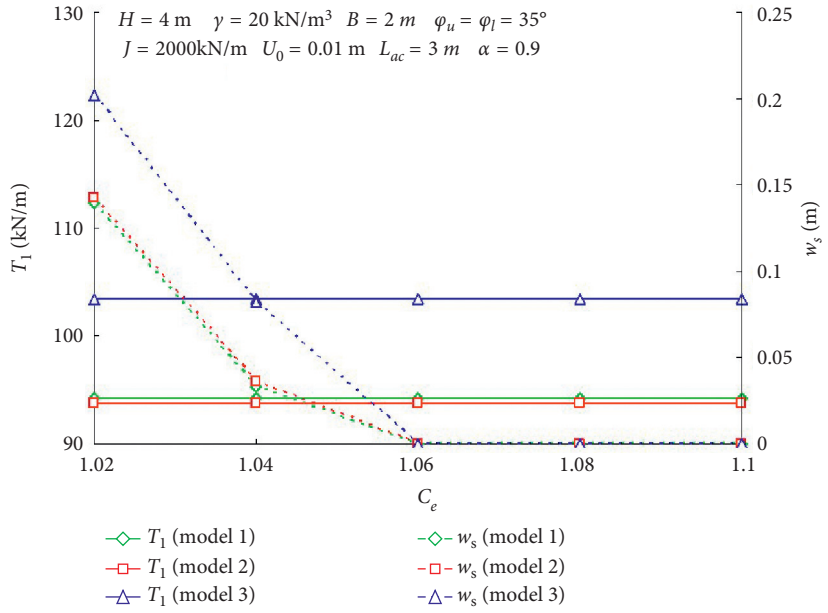

Figure 16: Influence of the expansion coefficient on the maximum tensile force and surface settlement.

$$\begin{cases} \text{if } U_A \le U_0\text{: } \dfrac{T_2}{Jr} = -+\dfrac{1}{12}B\left(\sqrt{4+\dfrac{Q^2}{{T_H}^2}}-\dfrac{Q^2}{10{T_H}^2}+\dfrac{Q^4}{96{T_H}^4}\right)-\dfrac{T_H}{J}\left(\dfrac{B}{2}+\dfrac{BQ^2}{40{T_H}^2}\right), \\ \text{if } U_A > U_0\text{: } U_0+\dfrac{{T_2}^2-{T_0}^2}{2J\tau_0} = -\dfrac{B}{6}+\dfrac{1}{12}B\left(\sqrt{4+\dfrac{Q^2}{{T_H}^2}}-\dfrac{Q^2}{10{T_H}^2}+\dfrac{Q^4}{96{T_H}^4}\right)-\dfrac{T_H}{J}\left(\dfrac{B}{2}+\dfrac{BQ^2}{40{T_H}^2}\right). \end{cases} \tag{36}$$

The solution for T_H from (36) is obtained by an iterative calculation. Determination together with equations (19), (20), and (26) makes it possible to calculate the maximum tensile force within the geosynthetic and surface settlement.

4. Analysis of Reinforced Embankment Bridging a Circular Void

As for general reinforced materials, such as woven geotextiles and geogrids, they usually have different tensile characteristics in the two principal directions. It is necessary to consider the anisotropy of geosynthetics when they are used for circular voids. However, Gourc and Villard [5] illustrated that unidirectional geosynthetics placed with machine direction along the direction of traffic are the most appropriate types. Hence, it is essential to analyze the cases that unidirectional reinforcement is used to bridge circular voids. A conservative approach can be applied to analyze these cases. It is assumed that a long void with a width, B, equal to the diameter, D, of the circular void was used to replace the circular void for mechanical analyses and the transverse tensile strength of the geosynthetic was neglected [11]. The analysis procedure for the circular void will be the same as the long void. Figure 17 presents the schematic diagram of the vertical load distribution on the geosynthetic layer spanning a circular void.

4.1. Geosynthetic Behavior in the Collapse Area. The vertical load can be written as

$$q(x) = \frac{12Q}{\pi D^3}x. \tag{37}$$

Combining (15) and (37), the expression obtained is

$$z = -\frac{2Q}{\pi T_H D^3}x^3 + \frac{Q}{4\pi T_H}. \tag{38}$$

From (38), we obtain

$$T_1 = \sqrt{{T_H}^2+\left(\frac{3Q}{2\pi D}\right)^2}. \tag{39}$$

$$w = \frac{Q}{4\pi T_H}. \tag{40}$$

If $w/D < 1/6$, the displacement of point A U_A can be written as

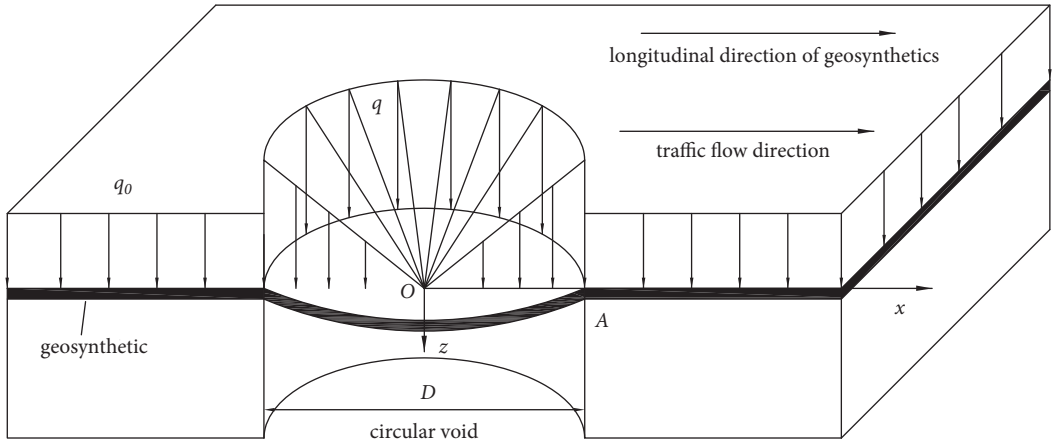

Figure 17: Schematic diagram of the vertical loads on geosynthetic spanning a circular void.

$$U_A = -\left(\frac{D}{6}\right) + \frac{1}{12}D\left(\sqrt{4+9\lambda^2} - \frac{3}{4}\lambda^2 + \frac{27}{32}\lambda^4\right) - \frac{T_H}{J}\left(\frac{D}{2} + \frac{9D}{40}\lambda^2\right), \tag{41}$$

where $\lambda = Q/(\pi D T_H)$.

4.2. Surface Settlement. Assuming that the shape of surface settlement and the geosynthetic sag are both cubical parabola of revolution, combined with (40), the relation among surface settlement w_s, deflection of geosynthetic w, soil expansion coefficient C_e, and height of the fill H can be obtained.

$$w_s = w\left[1 - \frac{20\pi T_H}{3Q}H\left(C_e - 1\right)\right]. \tag{42}$$

4.3. Geosynthetic Behavior in the Anchorage Area. The comparison between two-dimensional (2D) and three-dimensional (3D) trapdoor experiments demonstrates that the vertical stress on the fixed support in 3D trapdoor experiments increases by a much smaller amount than that in 2D [17]. Thereafter, consideration of the increments of the vertical stress in anchorage areas for circular voids is unnecessary. The relationship between U_A and T_2 can be determined by equation (35).

4.4. Analytical Formulation. Combining (35) and (41), the solution of the system is

$$\begin{cases} \text{if } U_A \le U_0\text{: } \dfrac{T_2}{Jr} = -\dfrac{D}{6} + \dfrac{1}{12}D\left(\sqrt{4+9\lambda^2} - \dfrac{3}{4}\lambda^2 + \dfrac{27}{32}\lambda^4\right) - \dfrac{T_H}{J}\left(\dfrac{D}{2} + \dfrac{9D}{40}\lambda^2\right), \\ \text{if } U_A > U_0\text{: } U_0 + \dfrac{T_2^{\,2} - T_0^{\,2}}{2J\tau_0} = -\dfrac{D}{6} + \dfrac{1}{12}D\left(\sqrt{4+9\lambda^2} - \dfrac{3}{4}\lambda^2 + \dfrac{27}{32}\lambda^4\right) - \dfrac{T_H}{J}\left(\dfrac{D}{2} + \dfrac{9D}{40}\lambda^2\right). \end{cases} \tag{43}$$

The solution for T_H from (43) is obtained by an iterative calculation. The maximum tensile force T_1 and the surface settlement w_s can be determined by (39) and (42).

5. Design Chart

The reinforcement must satisfy the requirement of the ultimate state and the serviceability limit state of the geosynthetic-reinforced embankment. That is, the maximum tensile force T_1 is lower than the acceptable tensile force T_{adm} of the geosynthetic and the maximum surface settlement w_s is less than the allowable surface settlement w_c. Design charts are established from the derivations presented in Sections 3 and 4. These charts present the maximum tensile force and surface settlement for given parameters. Inadvertent changes in embankment height and properties of fill for designed transport routes occur in engineering practice. Therefore, the geosynthetic stiffness is determined to be the main factor in the consideration. Generally, there is a positive correlation between the tensile stiffness (J) and strength (T_c) of the geosynthetic.

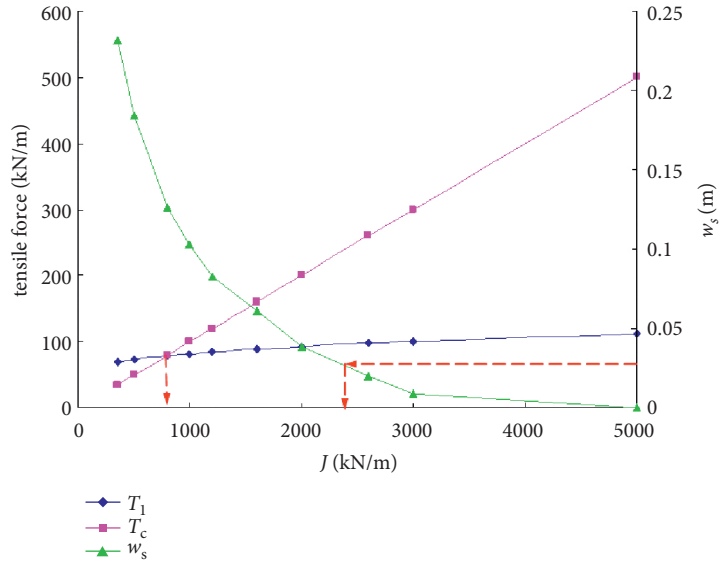

Figure 18: Chart for a long void.

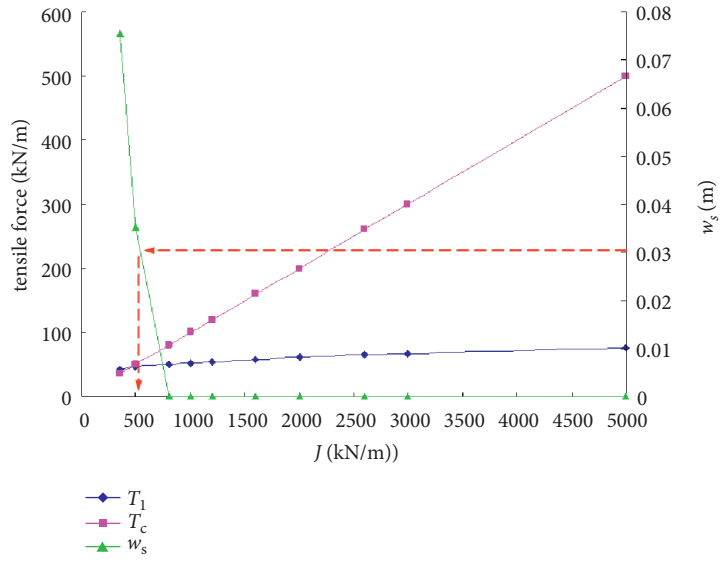

Figure 19: Chart for a circular void.

It is assumed that $T_c = 0.1J$ and $q_0 = \gamma H$ in the following examples. Charts for long and circular voids are plotted to find proper values of J complying with the surface settlement and tensile force criteria ($w_s < w_c$ and $T_1 < T_{adm}$). These charts are prepared without any safety factors and strength reduction factors of geosynthetics due to creep, damage during construction, connections, environmental impacts, etc. (i.e., $T_{adm} = T_c$).

Long void.

$B = 2\ m$, $H = 4\ m$, $\varphi_u = \varphi_l = 35°$, $\gamma = 20\ \text{kN/m}^3$, $U_0 = 0.01\ m$, $C_e = 1.04$, $w_c = 0.03\ m$, and $\alpha = 0.9$.

In the example presented in Figure 18, for criteria $w_s < 0.03\ m$ and $T_1 < T_c$, we determine the minimum geosynthetic stiffness: $J = 2400$ kN/m.

Circular void.

$D = 2\ m$, $H = 4\ m$, $\varphi_u = \varphi_l = 35°$, $\gamma = 20\ \text{kN/m}^3$, $U_0 = 0.01\ m$, $C_e = 1.04$, $w_c = 0.03\ m$, and $\alpha = 0.9$.

The same design procedure can be applied to a circular void. From Figure 19, we determine the minimum geosynthetic stiffness: $J = 500$ kN/m.

6. Conclusions

This study proposes a new analytical method to consider the 'secondary arching effect' and the resultant distribution of vertical loads acting on the unidirectional geosynthetic in the anchorage area. It is argued that the distribution of vertical stress on the geosynthetic in the anchorage area for a long void and $H/B = 1 \sim 4$ could be approximately described by a Gaussian function. The existing analysis methods were

modified by replacing a uniform vertical load distribution with an inverse triangular vertical load distribution in the collapse area. The differential method was adopted to analyze the geosynthetic in the anchorage area. Analytical equations and design charts were proposed based on the assumptions that an inverse triangular vertical load acts on the geosynthetic in the collapse area and the vertical uniform load on the geosynthetic in the anchorage area corresponding to the geostatic stress. The increment of vertical load in the anchorage area is neglected and the arching effect within cohesive soils is also investigated. The salient findings of this study are summarized as follows:

(i) The results of three calculation models indicated that the increment of vertical load in the anchorage area has little influence on the maximum tensile force and surface settlement if the anchorage length is long enough. For a situation with a short necessary anchorage length, this will be different when the minimum necessary anchorage length is several meters.

(ii) The vertical load distribution on geosynthetic in the collapse area has a significant effect on the maximum tensile force and surface settlement. A uniform vertical load distribution on the geosynthetic in the collapse area will overestimate the maximum tensile force and surface settlement, leading to economic waste. By contrast, the proposed inverse triangular distribution on the geosynthetic in the collapse area will cause rather small results which are also accepted. It is economical to adopt an inverse triangular distribution on the geosynthetic in the collapse area for engineering interests.

(iii) Due to uncertain changes in embankment height and properties of fill, a new design method is presented to determine the minimum geosynthetic stiffness to meet design standards. The minimum geosynthetic stiffness can be obtained by not allowing the maximum tensile force and surface settlement, calculated by specific parameters of geosynthetic reinforcement to exceed the allowable threshold.

Abbreviations

B: Cavity width (m)
C_e: Expansion coefficient of the fill soil
D: Cavity diameter (m)
H: Fill soil thickness (m)
J: Geosynthetic stiffness (kN/m)
K: Coefficient of lateral Earth pressure
K_a: Earth pressure coefficient
L_{ac}: Anchorage length (m)
q: Vertical load on the geosynthetic in the collapse area or on the yielding support in the trapdoor experiment (kPa)
Q: Total vertical force on the geosynthetic in collapse area or on the yielding support in the trapdoor experiment (kN)
q_s: Vertical overload applied on the fill soil surface (kPa)
q_a: Vertical load on the geosynthetic in anchorage area or on the fixed support in the trapdoor experiment (kPa)
q_0: Initial vertical load on the geosynthetic or on the support in the trapdoor experiment (kPa)
T: Tensile force within the geosynthetic (kN/m)
T_1: The maximum tensile force within the geosynthetic (kN/m)
T_2: Decreased tensile force within the geosynthetic at the edge of the void (kN/m)
T_{ac}: Tensile force within the geosynthetic without arching effect (kN/m)
T_c: Strength of the geosynthetic (kN/m)
T_{adm}: Accepted tensile force of the geosynthetic (kN/m)
T_H: Horizontal component force of the tensile force within the geosynthetic (kN/m)
T_V: Vertical component force of the tensile force within the geosynthetic (kN/m)
U_0: Relative displacement from which the friction mobilization becomes maximum (m)
U_A: Displacement of the geosynthetic at the point A (m)
U_{ak}: Displacement of the geosynthetic at any point (m)
w: Deflection of the geosynthetic (m)
w_s: The maximum surface settlement (m)
w_c: Allowable surface settlement (m)
x: Distance from the centerline of the void or trapdoor (m)
z: Vertical displacement of the geosynthetic (m)
α: Frictional coefficient
ΔL: Increase in geosynthetic length on the half-width of the cavity (m)
χ: Tension deformation in geosynthetic on the half-width of the cavity (m)
φ_u: Angle of internal friction of the fill soil (°)
φ_l: Angle of internal friction of the foundation soil (°)
γ: Unit weight of fill soil (kN/m^3)
ε: Geosynthetic strain
σ: Parameter in the Gaussian function
σ_n: Normal stress applied on the interface, $\sigma_n = q_a$ in the anchorage area (kPa)
τ_u: Friction stress at the upper interface between soil and geosynthetic (kPa)
τ_l: Friction stress at the lower interface between soil and geosynthetic (kPa).

Data Availability

Some or all data, models, or codes generated or used during the study and the experimental data used to support the findings of this study are available from the corresponding author by request.

Conflicts of Interest

The authors declare that they have no conflicts of interest.

Acknowledgments

The research has been sponsored by the Shanghai Rising-Star Program of China (18QB1403800).

References

[1] S. J. Feng, S. G. Ai, and H. X. Chen, "Estimation of arching effect in geosynthetic-reinforced structures," *Computers and Geotechnics*, vol. 87, pp. 188–197, 2017.

[2] F. Lai, F. Chen, and D. Li, "Bearing capacity characteristics and failure modes of low geosynthetic-reinforced embankments overlying voids," *International Journal of Geomechanics*, vol. 18, no. 8, Article ID 04018085, 2018.

[3] Y. Zhou, F. Chen, and Y. Lin, "Solution for low geosynthetic-reinforced embankments subjected to localized sinkholes," *Soil Mechanics and Foundation Engineering*, vol. 56, no. 1, pp. 28–36, 2019.

[4] T. C. Kinney and B. Connor, "Geosynthetics supporting embankments over voids," *Journal of Cold Regions Engineering*, vol. 1, no. 4, pp. 158–170, 1987.

[5] J. Gourc and P. Villard, "Reinforcement by membrane effect: application to embankments on soil liable to subsidence," in *Proceedings of the 2nd Asian Geosynthetics Conference*, Seoul, Korea, June 2000.

[6] P. Villard, J. P. Gourc, and H. Giraud, "A geosynthetic reinforcement solution to prevent the formation of localized sinkholes," *Canadian Geotechnical Journal*, vol. 37, no. 5, pp. 987–999, 2000.

[7] P. Villard and L. Briançon, "Design of geosynthetic reinforcements for platforms subjected to localized sinkholes," *Canadian Geotechnical Journal*, vol. 45, no. 2, pp. 196–209, 2008.

[8] A. Elshesheny, M. Mohamed, and T. Sheehan, "Buried flexible pipes behaviour in unreinforced and reinforced soils under cyclic loading," *Geosynthetics International*, vol. 26, no. 2, pp. 184–205, 2019.

[9] W. Lu, L. Miao, E. Wang, J. Zhang, Y. Zhang, and H. Wang, "A case study on geogrid-reinforced and pile-supported widened highway embankment," *Geosynthetics International*, vol. 27, no. 3, pp. 261–274, 2020.

[10] Q. A. Tran, P. Villard, and D. Dias, "Geosynthetic reinforced piled embankment modeling using discrete and continuum approaches," *Geotextiles and Geomembranes*, vol. 49, no. 1, pp. 243–256, 2021.

[11] J. P. Giroud, R. Bonaparte, J. F. Beech, and B. A. Gross, "Design of soil layer-geosynthetic systems overlying voids," *Geotextiles and Geomembranes*, vol. 9, no. 1, pp. 11–50, 1990.

[12] J. C. Blivet, J. P. Gourc, P. Villard, H. Giraud, M. Khay, and A. Morbois, "Design method for geosynthetic as reinforcement for embankment subjected to localized subsidence," in *Proceedings of the 7th International Conference On Geosynthetics*, vol. 1, pp. 341–344, Nice, France, September 2002.

[13] J. A. Sloan, *Column-supported embankments: full-scale tests and design recommendations*, Ph.D. Thesis, Virginia Polytechnic Institute and State University, Blacksburg, VA, USA, 2011.

[14] S. J. M. van Eekelen, A. Bezuijen, H. J. Lodder, and A. F. Van Tol, "Model experiments on piled embankments. Part II," *Geotextiles and Geomembranes*, vol. 32, no. 1, pp. 82–94, 2012.

[15] S. J. M. Van Eekelen, A. Bezuijen, and A. F. Van Tol, "An analytical model for arching in piled embankments," *Geotextiles and Geomembranes*, vol. 39, pp. 78–102, 2013.

[16] T. S. da Silva Burke and M. Z. E. B. Elshafie, "Geosynthetic-reinforced soils above voids: observation and prediction of soil arching," *Geotextiles and Geomembranes*, vol. 49, no. 3, pp. 579–592, 2021.

[17] T. Adachi, M. Kimura, and K. Kishida, "Experimental study on the distribution of earth pressure and surface settlement through three-dimensional trapdoor tests," *Tunneling and Underground Space Technology incorporating Trenchless Technology Research*, vol. 18, no. 2-3, pp. 171–183, 2003.

[18] R. Jia, "*Study on relaxation effect of vertical soil pressure for shield tunnel*," M.S. Thesis, Hohai University, Hohai, China, 2007.

[19] D. Gao, *Deformation and stability of intermediate liner for landfill expansion and controlling measures*, Ph.D. Thesis, Zhejiang University, China, 2009.

[20] R. Rui, F. van Tol, X. L. Xia, S. van Eekelen, G. Hu, and Y. Y. Xia, "Evolution of soil arching; 2D DEM simulations," *Computers and Geotechnics*, vol. 73, pp. 199–209, 2016.

[21] K. Terzaghi, *Theoretical Soil Mechanics*, John Wiley & Sons, Hoboken, NJ, USA, 1943.

[22] B. Chevalier, G. Combe, and P. Villard, "Experimental and discrete element modeling studies of the trapdoor problem: influence of the macro-mechanical frictional parameters," *Acta Geotechnica*, vol. 7, no. 1, pp. 15–39, 2012.

[23] L. Briançon and P. Villard, "Design of geosynthetic-reinforced platforms spanning localized sinkholes," *Geotextiles and Geomembranes*, vol. 26, no. 5, pp. 416–428, 2008.

[24] German Geotechnical Society, *Recommendations for Design and Analysis of Earth Structures Using Geosynthetic Reinforcements - EBGEO*, Wilhelm Ernst & Sohn, Berlin, Germany, 2nd edition, 2011.

[25] A. Bezuijen and S. J. M. V. Eekelen, "Basal reinforced piled embankments: validation of inverse triangular load 390 distribution with an extended terzaghi equation," in *Proceedings of the 10th International Conference on Geosynthetics*, ICG, Berlin, Germany, September 2014.

[26] S. J. Feng, S. G. Ai, and H. X. Chen, "Membrane effect of geosynthetic reinforcement subjected to localized sinkholes," *Canadian Geotechnical Journal*, vol. 55, no. 7, pp. 1334–1348, 2018.

[27] Bs, *Code of Practice for Strengthened/reinforced Soils and Other Fills*, pp. 179–191, British Standards Institution, Chiswick High Road, UK, 2010.